

**COORDINATED ISOTOPIC AND MINERAL CHARACTERIZATION OF HIGHLY FRACTIONATED  $^{18}\text{O}$ -RICH SILICATES IN THE QUEEN ALEXANDRA RANGE 99177 CR3 CHONDRITE.** A. N. Nguyen<sup>1,2</sup>, L. P. Keller<sup>2</sup>, S. Messenger<sup>2</sup>, and Z. Rahman<sup>1,2</sup>. <sup>1</sup>JETS JACOBS, NASA JSC, Houston TX. <sup>2</sup>Robert M. Walker Laboratory for Space Science, ARES, NASA JSC, Houston TX. lan-anh.n.nguyen@nasa.gov

**Introduction:** Carbonaceous chondrites contain a mixture of solar system condensates, presolar grains, and primitive organic matter. Each of these materials record conditions and processes in different regions of the solar nebula, on the meteorite parent body, and beyond the solar system. Oxygen isotopic studies of meteorite components can trace interactions of distinct oxygen isotopic reservoirs in the early solar system and secondary alteration processes. The O isotopic compositions of the earliest solar system condensates fall along a carbonaceous chondrite anhydrous mineral (CCAM) line of slope  $\sim 1$  in a plot of  $\delta^{17}\text{O}$  against  $\delta^{18}\text{O}$ . This trend is attributed to mixing of material from  $^{16}\text{O}$ -poor and  $^{16}\text{O}$ -rich reservoirs [1]. Secondary processing can induce mass-dependent fractionation of the O isotopes, shifting these compositions along a line of slope  $\sim 0.52$ .

Substantial mass-dependent fractionation of O isotopes has been observed in secondary minerals in CAIs [2, 3], calcite [4, 5], and FUN inclusions [6]. These fractionations were caused by significant thermal or aqueous alteration. We recently reported the identification of four silicate grains with extremely fractionated O isotopic ratios ( $\delta^{18}\text{O} = 37 - 55\text{‰}$ ) in the minimally altered CR3 chondrite QUE 99177 [7]. TEM analysis of one grain indicates it is a nebular condensate that did not experience substantial alteration. The history of these grains is thus distinct from those of the aforementioned fractionated materials. To constrain the origin of the silicate grains, we conducted further Mg and Fe isotopic studies and TEM analyses of two grains.

**Experimental:** A silicate-rich separate of matrix grains  $\sim 0.5 - 2\text{ }\mu\text{m}$  from the QUE 99177 meteorite was produced by gentle disaggregation and centrifugation. These grains were deposited from liquid suspension onto Au foil. Four  $^{18}\text{O}$ -rich grains were identified by raster ion imaging of the O and Si isotopes and  $^{27}\text{Al}^{16}\text{O}$  in the JSC NanoSIMS 50L. The O isotopic ratios of these grains were re-measured and confirmed. TEM analysis of a focused ion beam (FIB) produced cross-section of grain 13\_5 ( $\sim 3 \times 7\text{ }\mu\text{m}$ ) was conducted. Grains 11\_2 and 14\_7 were analyzed further for  $^{24}\text{Mg}$ ,  $^{25}\text{Mg}$ ,  $^{26}\text{Mg}$ , and  $^{27}\text{Al}$  by raster ion imaging using a  $\sim 6.5\text{ pA O}^-$  primary beam. These two grains were then analyzed for  $^{54}\text{Fe}$ ,  $^{56}\text{Fe}$ ,  $^{57}\text{Fe}$ , and  $^{52}\text{Cr}$  with a  $\sim 10\text{ pA O}^-$  primary beam. The  $^{54}\text{Cr}$  interference on  $^{54}\text{Fe}$  was corrected for by assuming the grains had solar  $^{54}\text{Cr}/^{52}\text{Cr}$  isotopic ratios. All isotopic ratios are normalized to the neighboring matrix grains within the image map.

Electron transparent sections of grains 11\_2 ( $\sim 3 \times 5\text{ }\mu\text{m}$ ) and 14\_7 ( $\sim 8 \times 11\text{ }\mu\text{m}$ ) were produced by FIB milling and lift-out in the same manner as grain 13\_5. Electron beam deposited C was placed across the grains followed by ion beam deposited C straps over the entire length of the sections. The grain chemistry and mineralogy were obtained with the JSC JEOL 2500 field-emission scanning TEM. Elemental maps were acquired with a Noran thin window EDX spectrometer. The structure of the grains was determined by electron diffraction and dark-field imaging.

**Results: Isotopic analyses.** The four grains have moderate  $^{18}\text{O}$ -enrichments ( $\delta^{18}\text{O} = 37 - 55\text{‰}$ ) but normal  $^{17}\text{O}/^{16}\text{O}$  ratios within error (Fig. 1). Their O isotopic ratios fall within  $2\sigma$  of the terrestrial fractionation line with the average  $\Delta^{17}\text{O} = -11 \pm 18\text{‰}$  ( $2\sigma$  error). The Si isotopic ratios of all four grains and the Fe isotopic ratios of grains 11\_2 and 14\_7 fall within the range observed for the surrounding matrix. The Mg isotopic ratios of 11\_2 and 14\_7 fall on a mass-dependent fractionation line with no detection of excess  $^{26}\text{Mg}$ . The Mg isotopic ratios are within the range measured for the matrix grains.

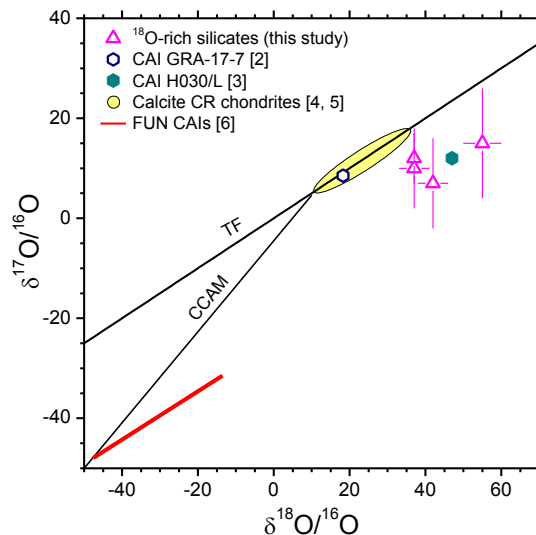


Figure 1. Oxygen isotopic ratios of highly fractionated silicates and fractionated secondary phases.  $1\sigma$  errors.

**Chemical and mineral characterization.** 13\_5 is an aggregate of two platy pyroxene grains of the same orientation (Fig. 2). Exsolution lamellae of Ca-rich pyroxene occur on the top surface of and within the upper enstatite grain. This enstatite has wt.% levels of transition elements with  $\text{Cr} + \text{Mn} > \text{Fe}$ , similar to low-Fe, Mg-enriched “LIME” olivines and pyroxenes found in IDPs

(Klöck et al. 1989). The lower grain is homogeneous high-Ca pyroxene. The pyroxene grains are surrounded by a thin layer of fine-grained Fe-rich olivine that has FeNi metal and chromite inclusions.

The surface of 14\_7 appeared smooth after the initial NanoSIMS analysis but became more porous and pitted after subsequent isotopic analyses. TEM characterization of the cross-section shows the entire grain is very porous. The bulk of the material is a mixture of amorphous Fe-rich silicate and nanocrystalline Fe-rich oxide with minor Ni (Fig. 3). Several crystalline grains are embedded within this groundmass. Grain 1 in Figure 3 is a crystalline plagioclase grain of composition An<sub>75</sub>Ab<sub>25</sub> (75% CaAl<sub>2</sub>Si<sub>2</sub>O<sub>8</sub>, 25% NaAlSi<sub>3</sub>O<sub>8</sub>). Grain 2 is an enstatite grain with trace Mn, Cr, and Fe and an FeNi inclusion. Grain 3 is a Mg-rich olivine (Fo<sub>95</sub>).

The composition and texture of grain 11\_2 (Fig. 4) is very similar to 14\_7. Most of the material is Fe-rich nanocrystalline Fe-Ni oxides in an amorphous silicate matrix. Grain 1 in Figure 4 is an amorphous stoichiometric Mg-rich olivine (Fo<sub>95</sub>) that was likely amorphized during isotopic analysis. Grain 2 is a crystalline enstatite with a small adjoining diopside grain.

**Discussion:** The O isotopic compositions of the silicate grains are quite unusual. Large O isotope fractionation has been observed in calcite grains and rare refractory inclusions (Fig. 1). For the calcite grains [4, 5] and CAI GRA-17-7 [2], these fractionations are attributed to aqueous alteration. The FUN CAIs [6] and the unusual hibonite-rich CAI H030/L [3] likely formed by melting and partial evaporation of <sup>16</sup>O-rich precursors.

Though the O isotopic compositions of the silicates in this study are similar to CAI H030/L, it is unlikely that evaporative loss or aqueous alteration caused the observed fractionation of O. The platy morphology of the pyroxene and trace element enrichments of grain 13\_5 advocate a condensation origin with no subsequent alteration. The texture of the Fe-rich olivine layers and the exsolution within the pyroxene are consistent with formation at ~1400 K. The crystalline silicates in grains 14\_7 and 11\_2 do not have equilibrated grain boundaries and could be direct condensates similar to 13\_5. The amorphous silicate matrix does not show extensive alteration (i.e., no phyllosilicates) and could be non-equilibrium nebular condensates akin to GEMS (glass with embedded metal and sulfides) grains that were oxidized and mildly hydrated on the parent body. Similarly, studies of primitive carbonaceous chondrites indicate the amorphous silicate precursors were likely GEMS grains that experienced parent body alteration [8, 9].

As the grains in this study were not extensively altered, they most likely acquired their fractionated O compositions by direct condensation from an <sup>18</sup>O-rich

gas reservoir. We speculate that the grain precursor materials were CAI-like with initial  $\delta^{17,18}\text{O} \sim -50\text{‰}$ . This material then underwent isotopic exchange with a <sup>16</sup>O-poor reservoir, shifting their compositions up the CCAM line to  $\delta^{18}\text{O} \sim -15\text{‰}$ . Subsequent heating and evaporation of this material fractionated the O isotopes to  $\delta^{18}\text{O} \sim 45\text{‰}$ . Complete evaporation of this fractionated material produced the <sup>18</sup>O-rich gas reservoir from which the silicates condensed. This <sup>18</sup>O-rich reservoir might be expected to also have fractionated Mg, Fe, and Si isotopes, yet this fractionation is not observed in the silicates. CAI H030/L also has isotopically normal Mg and it was proposed that nearly all Mg was lost during heating of the precursors [3]. Thus, the <sup>18</sup>O-rich gas reservoir did not have Mg, Fe, or Si from the precursor. The silicates likely acquired isotopically normal Mg, Fe, and Si from the surrounding gas and perhaps through equilibration on the parent body. We will search for additional fractionated grains to constrain their origins.

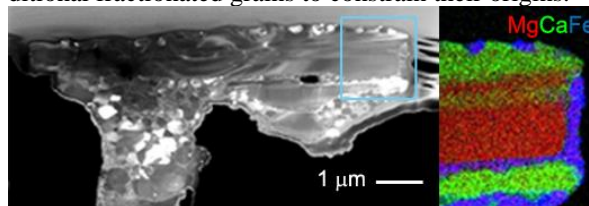


Figure 2. Dark-field STEM image of section 13\_5 and elemental map of outlined region.

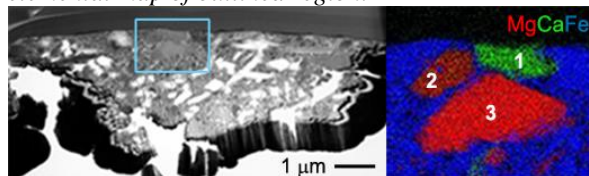


Figure 3. Bright-field STEM image of 14\_7 and elemental map of outlined region containing crystalline grains encapsulated in the amorphous silicate matrix.

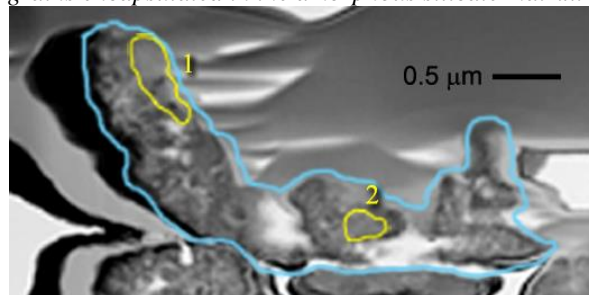


Figure 4. Bright-field STEM image of 11\_2 bounded in blue, with crystalline grains 1 and 2 outlined in yellow.

**References:** [1] McKeegan K.D. et al. (2011) *Science*, 332, 1528. [2] Aléon J. et al. (2002) *MAPS*, 37, 1729. [3] Rout S.S. et al. (2009) *GCA*, 73, 4264. [4] Keller L.P. et al. (2012) *43<sup>rd</sup> LPSC*, #2065. [5] Jilly-Rehak C.E. et al. (2015) *46<sup>th</sup> LPSC*, #1662. [6] Krot A.N. et al. (2010) *ApJ*, 713, 1159. [7] Nguyen A.N. et al. (2015) *MAPS*, 50, A5386. [8] Nakamura-Messenger K. et al. (2011) *MAPS*, 46, 843. [9] Keller L.P. and Messenger S. (2012) *43<sup>rd</sup> LPSC*, 43, #1880.